# PIXEL INTENSITY DISTRIBUTION MODELS FOR FILTERED BACK-PROJECTION

J-P. GUEDON[1], M. UNSER[2], Y. BIZAIS[3]
[1] Center for Devices and Radiological Health, FDA, Rockville, MD
[2] Biological Engineering and Instrumentation Program, NIH, Bethesda,MD
[3] Imagerie Medicale Multimodalite, University Hospital, Nantes, France

*Abstract*

We define a Pixel Intensity Distribution Model (PIDM) to study the discretization of direct reconstruction schemes in a proper way. For the Filtered BackProjection (FBP) algorithm, this leads to a derivation of the filter for a B-spline PIDM and its discretization, a simple but exact implementation for this class of functions, and a rule for the sampling ratio relating pixel size to projection cell size according to the device characteristics. Actual phantom reconstructions are presented both for standard and spline FBP schemes. The degree of the B-spline reconstruction is discussed in connection with the angular sampling and the kind of detection task to be applied on the image.

## I. INTRODUCTION

The filtered backprojection (FBP) is a technique widely used for tomographic reconstruction. In order to regularize the Ramp filter, only low frequencies are kept in the algorithm through the use of a so-called apodisation window. The obtained reconstruction is then a band-limited approximation of the original function. In this paper we will use the space of B-spline functions to derive a new algorithm. In the second section, we will present the derivation of the regularized Ramp filter for the the standard band-limited approximation and for $V_0(IR^2)$, the space of piecewise constant functions. Using this latter space corresponds to assuming a constant Pixel Intensity Distribution Model (PIDM), also called Haar system in the literature. In section III, we will generalize this approach to the class of B-spline PIDM with the use of spaces $V_n(IR^2)$ composed by polynomial splines of degree n. We will discuss in section IV the applications and limitations of both approaches for the evaluation of detection tasks.

## II. CONTINUOUS FBP AND DISCRETE REPRESENTATIONS

In this section, we derive the main formulas for the FBP reconstruction in S', and its application to the subspace of bandlimited functions and the B-spline space of degree 0 (Haar system). The proof of the Haar system reconstruction is explained in more details in [1]. The differences between classical bandlimited and spline reconstruction will be pointed out. We will also derive the discrete filter for $V_0$.

### *A. Continuous Reconstructions*

The continuous FBP reconstruction of a function $f(x,y) \in S'$ (the space of tempered distributions) from its projections $p_f(t,\theta)$ is well understood theorically [10]. This process can be described by the following identity:

$$f(x,y) = R^* K R\ f(x,y) = R^* K\ p_f(t,\theta)\ , \tag{1}$$

where the operators $R^*$, $K$ and $R$ are defined as follows. The projections $p_f(t,\theta)$ of $f(x,y)$ (with $t = x\cos\theta - y\sin\theta$) are obtained by the Radon operator $R$:

$$R\ [f(x,y)] = p_f(t,\theta) \tag{2}$$

$$p_f(t,\theta) = \int_{-\infty}^{+\infty}\int_{-\infty}^{+\infty} f(x,y)\ \delta(t - x\cos\theta + y\sin\theta)\ dx dy\ .$$

The operator $K$ represents the filtering part of the algorithm in which each projection is convolved with the inverse Fourier transform of the infinite Ramp:

$$K\ p_f(t,\theta) = \tilde{p}_f(t,\theta) = p_f(t,\theta) * F_1^{-1}\ [\pi|\nu|]\ . \tag{3}$$

The backprojection (BP) operator $R^*$ is the dual operator of $R$ and is defined by:

$$R^*\ \left[\tilde{p}_f(t,\theta)\right] = f\ (x,y) = \frac{1}{\pi}\int_0^{\pi} \tilde{p}_f(t,\theta)\ d\theta\ . \tag{4}$$

These results apply for the reconstruction of functions of the continuous variables x and y. What one is seeking in practice is a discrete implementation of this algorithm. For this purpose, we consider the standard approach to the discretization of a function $f(x,y)$ which consists of applying a prefilter to the image and sampling thereafter

$$\hat{f}_{k,l} = b\ (x,y)\ **\ f(x,y)\ \Big|_{\substack{x=k\\y=l}}\ . \tag{5}$$

The sampling kernel $b(x,y)$ is an anti-aliasing filter such as, for example, the ideal lowpass filter dictated by Shannon sampling theorem.

We will now start from this latter equation and use the continuous FBP reconstruction scheme (1) in order to derive the discrete version of this algorithm. It is not difficult to show that we have the following identity for the non-sampled version of (5):

$$b\ **f = R^* K\ (p_b\ * p_f)\ . \tag{6}$$

In other words, the 2D convolution of functions $b$ and $f$ is the reconstruction of the 1D convolution of their projections $p_f$ and $p_g$. After sampling this last equation, we obtain the general form of the discrete reconstruction algorithm

$$\hat{f}_{k,l} = R^* K\ \left(p_b(t,\theta) * p_f(t,\theta)\right)\Big|_{\substack{x=k\\y=l}}\ . \tag{7}$$

Further, we can combine the infinite ramp and the projection of the sampling kernel in a single filter, which yields

$$\hat{f}_{k,l} = R^*\ \left(k\ (t,\theta) * p_f(t,\theta)\right)\Big|_{\substack{x=k\\y=l}}\ , \tag{8}$$

0-7803-0513-2/92$0.3.00 ©IEEE

where the filter $k(t,\theta)$ is given by:

$$k(t,\theta) = F_1^{-1}\left(\pi|\nu|\ P_b(\nu,\theta)\right), \tag{9}$$

and $P_b$ is the Fourier transform of $p_b$. Note that $k(t,\theta)$ is a function of the angle $\theta$ in this formulation.

Eq. (9) summarizes the continuous-discrete FBP algorithm for all PIDM representations. We will now consider some examples. First, we will show that this algorithm includes the standard procedure as a particular case. We will then apply it to the case of polynomial splines of degree zero (piecewise constant functions).

The common adopted solution for FBP combines a lowpass window (called apodisation window $A(\nu)$) with the infinite ramp filter, for example the Ram-Laks, Shepp-Logan, Butterworth, Haming filters. The standard filter in (9) reduces to:

$$k_s(t) = F_1^{-1}(\pi|\nu|A(\nu)). \tag{10}$$

This is in effect equivalent to choosing a particular sampling kernel in (5). The link with our formalism is provided by the formula

$$b(x,y) = H^{-1}(A(\nu)), \tag{11}$$

where $H$ is the Hankel transform (2D Fourier transform for rotational symetric functions). Instead of choosing a rotationally symetric function for the sampling kernel, we will now present the simplest separable case : the Haar system.

## B. Reconstruction in $V_0$ (IR $^2$)

Splines of degree zero are piecewise constant functions. They can be represented by the following formula

$$f_0(x,y) = \sum_{k=-\infty}^{+\infty}\sum_{l=-\infty}^{+\infty} f_0(k,l)\, s_{0,\Delta}(x-k, y-l), \tag{12}$$

where the basis functions, which define our PIDM, are

$$s_{0,\Delta}(x,y) = s_{0,\Delta}(x)\cdot s_{0,\Delta}(y), \tag{13}$$

These are simply obtained from the product of rectangular pulses of support $\Delta$ (the pixel size, in our case) along the x and y directions:

$$s_{0,\Delta}(z) = \begin{cases} 1 & \text{if } |z| < \Delta/2 \\ 1/2 & \text{if } |z| = \Delta/2 \\ 0 & \text{if } |z| > \Delta/2 \end{cases}. \tag{14}$$

The space of all $L_2$ functions of the form (12) is denoted by $V_0$ (IR $^2$). It has been shown [5] that the optimal prefilter for the projection of a function $f(x,y)$ in $V_0$ (IR$^2$) is also given by Eq. (13). Hence, Eq. (8) with $b(x,y)=s_{0,\Delta}(x,y)$ provides us with an algorithm for determining the coefficients $f_0(k,l)$ in (12) that best represent a function $f(x,y)$ in the least square sense; in other words, $f_0(x,y)$ is the least squares approximation of $f(x,y)$.

By using our previous results (Eqs (7) and (13)), we obtain the reconstruction algorithm:

$$f_0(k,l) = R^* K\left(w_0(t,\theta) * p_f(t,\theta)\right)\Big|_{\substack{x=k\\y=l}}. \tag{15}$$

where

$$w_0(t,\theta) = R\ s_{0,\Delta}(x,y), \tag{16}$$

The corresponding filter in the reconstruction algorithm (8) is:

$$k_0(t,\theta) = F_1^{-1}\left(\pi|\nu|W_0(\nu,\theta)\right), \tag{17}$$

where $W_0(\nu,\theta)$ is the Fourier transform of $w_0(t,\theta)$.

Computation of the Radon transform of the 2D Haar system basis defined in Eq. (13), leads to a generic trapezoidal function $w_0(t,\theta)$ depending on the angle $\theta$ [2]. Degenerate cases are a square for $\theta=0$ and a triangle for $\theta=\pi/4$. Another elegant way to express this function uses the Haar basis :

$$w_0(t,\theta) = s_{0,\Delta\cos\theta}(t) * s_{0,\Delta\sin\theta}(t), \tag{18}$$

since the Fourier transform of the trapezoidal function is a product of 2 sinc functions:

$$W_0(\nu,\theta) = \Delta^2\, sinc\,(\pi\nu\Delta\cos\theta)\, sinc\,(\pi\nu\Delta\sin\theta). \tag{19}$$

Therefore, the Fourier transform of $k_0(t,\theta)$ is:

$$K_0(\nu,\theta) = \Delta^2\pi|\nu|\ sinc\,(\pi\nu\Delta\cos\theta)\, sinc\,(\pi\nu\Delta\sin\theta). \tag{20}$$

Finally, the explicit formula for $k_0(t,\theta)$ is obtained by taking the inverse Fourier transform (for $t\neq0$ and $\theta\neq0$) which gives :

$$k_0(t,\theta) = \frac{1}{\pi\sin 2\theta}\ ln\left|\frac{t^2 - \frac{\Delta^2}{4}(1+\sin 2\theta)}{t^2 - \frac{\Delta^2}{4}(1-\sin 2\theta)}\right|. \tag{21}$$

## C. Differences between standard and Haar FBP

Clearly, the main difference between the standard and $V_0$ (IR $^2$) FBP algorithms is in the design of the filter $k(t,\theta)$. Most notably, the standard filter $k_s(t)$ is the same for all projections. In the spline case, it depends on the angle $\theta$. This difference will be especially noticeable for projection sampling.

1. Angular sampling. When the FBP scheme is implemented, only a finite number of projections are available. The Haar filter will take into account the respective position of the projection with respect to the pixel grid orientation. The underlying discrete image representation is not isotropic: this filter is then particularly adapted to the pixel representation because it depends on the size $\Delta$.

2. Linear sampling. The standard FBP is generally implemented with a cell size in the projections $\tau$ equals to the pixel size $\Delta$. This bandlimited reconstruction may exhibit aliasing [2],[3]. To reduce these artifacts, we have shown that an oversampling ratio $\rho$ between pixel size and projection cell size is needed :

$$\rho = \frac{\Delta}{\tau}. \tag{22}$$

For the Haar filter defined in (21), the oversampling ratio $\rho$ is also needed to ensure having enough knots in $w_0(t,\theta)$ to perform the convolution and not reduce this kernel to a delta function as it is the case for $\rho = 1$.

## D. Discrete filter values for $V_0$ (IR $^2$)

In practice, the derivation of the discrete filter values from (23) needs some special care because of potential singularities

at $n=0$ and $\theta=\pi/4$. Using the oversampling ratio $\rho$, the projection sampling is

$$t = n\,\tau = n\,\frac{\Delta}{\rho}, \tag{23}$$

and (21) is rewritten, for $n\neq 0$ and $\theta\neq 0$, as

$$k_0(n\,\frac{\Delta}{\rho},\theta) = \frac{1}{\pi \sin 2\theta}\; ln \left| \frac{\left(\frac{2n}{\rho}\right)^2 - 1 - \sin 2\theta}{\left(\frac{2n}{\rho}\right)^2 - 1 + \sin 2\theta} \right| . \tag{24}$$

For $n=0$ and/or $\theta=0$, the results are derived in [1] and summerized here. To avoid singularities, we have introduced the additional condition for $n=\rho/2$:

$$k_0(\frac{\Delta}{2},\theta) = 0\,, \tag{25}$$

This leads to the formulas

$$k_0(n\,\frac{\Delta}{\rho}, 0) = \frac{-2\rho^2}{\pi(4n^2 - \rho^2)}\,, \tag{26}$$

when $n\neq 0$ and $n\neq\rho/2$. The value at the origin depends directly on $\rho$ :

$$k_0(0,0) = \frac{2}{\pi}\; if\; \rho = 1\,, \tag{27}$$

$$k_0(0,0) = \frac{3}{\pi}\; if\; \rho = 2p,\; p\; integer$$

For n=0, the central value of the regularized filter is :

$$k_0(0,\theta) = \frac{2}{\pi \sin 2\theta}\; ln \left| \frac{sinc\,(\frac{\pi\rho}{2}\sqrt{1 - \sin 2\theta})}{sinc\,(\frac{\pi\rho}{2}\sqrt{1 + \sin 2\theta})} \right| . \tag{28}$$

which is in agreement with (21) when $\theta$ goes to zero. This last formula ensures both the numerical stability of the filter for $\theta=\pi/4$ and the zero gain of the filter at $\nu=0$ [1].

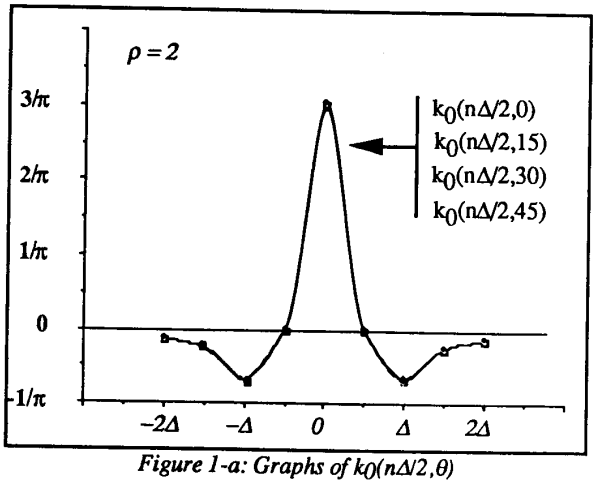


*Figure 1-a: Graphs of $k_0(n\Delta/2,\theta)$*

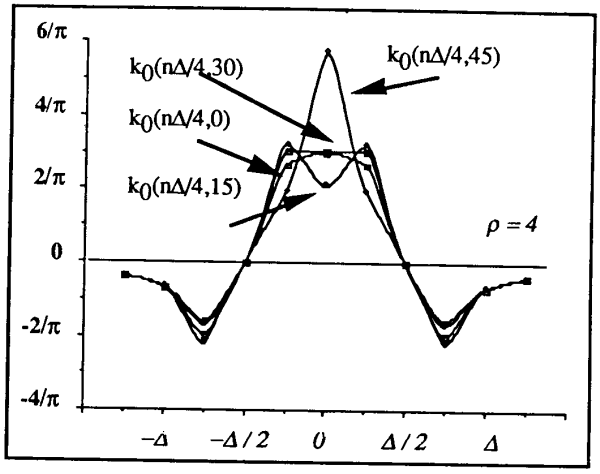


*Figure 1-b: Graphs of $k_0(n\Delta/4,\theta)$*

Figure 1 shows the impulse response of this filter for $\rho=2$ and 4 and for some values of $\theta$ which examplify the role of the oversampling ratio and the angular dependance.
For $\rho=2$ (Figure 1-a), the differences in the filter values are too small to be perceived on the graph which looks very much like the Shepp and Logan Ramp filter. At the opposite, for $\rho=4$ (Figure 1-b), we clearly see the angular dependances for each value of $\theta$. Especially for 0, we see the regularization effect of Eq. (28) whereas for $\theta = 15$ degrees, the central value of the filter decreases.

## III. $V_n(IR^2)$ PIDM

### A. $V_n\,(IR^2)$ basis functions and implementation

To generalize our approach to splines of higher degree, we will use the results of [4],[5] . Equation (5) may be used to represent the prefiltering and sampling operations of the Figure 2. This block diagram describes a computational solution for obtaining the projection of the function $f(x,y)$ onto $V_n\,(IR^2)$ (the space of polynomial splines of degree n). One notable difference is that the sampled coefficients in this block diagram are now different from the sampled value of the spline image; i.e, $C_{k,l} \neq f_n(k,l)$, $n>0$.

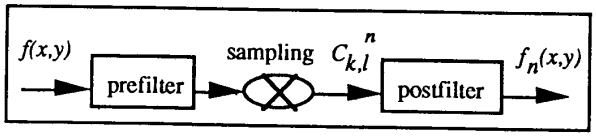


*Figure 2: Construction of $f_n(x,y)$ from $f(x,y)$*

In the dual spline representation, the prefilter is the 2D B-spline of degree n which can be defined by the classical recurrence relationship:

$$s_{n,\Delta}(x,y) = s_{n-1,\Delta}(x,y) * s_{0,\Delta}(x,y)\,, \tag{29}$$

Note that this sampling function is not confined into the pixel, but extended to its neighbours : it has a support length (n+1)Δ. The reconstruction of the continuous function is obtained by

$$f_n(x,y) = \sum_{k=-\infty}^{+\infty} \sum_{l=-\infty}^{+\infty} C_{k,l}^{n} \, \beta_{n,\Delta}(x - k, y - l) . \qquad (30)$$

The basis functions are obtained from the dual spline (D-spline) $\overset{o}{s}_{n,\Delta}(x,y)$ defined by:

$$\beta_{n,\Delta}(x,y) = \sum_{k=-\infty}^{+\infty} \sum_{l=-\infty}^{+\infty} \left(s_{2n+1,\Delta}\right)^{-1}(k,l) \, s_{n,\Delta}(x - k, y - l) , \qquad (31)$$

where $(.)^{-1}$ denotes the discrete convolution inverse. For more details, see [5].

By applying the results of Section 2.B, we get the following reconstruction algorithm for the D-spline coefficients in (30):

$$C_{k,l}^{n} = R^{*}\left( p(t,\theta) * k_0(t,\theta) * w_{n-1}(t,\theta) \right)\Big|_{\substack{x=k \\ y=l}} , \qquad (32)$$

with the same recurrent relationship for the kernel $w_n$ than for the basis function itself:

$$w_n(t,\theta) = w_{n-1}(t,\theta) * w_0(t,\theta) . \qquad (33)$$

By using an additional postfiltering step, we can obtain the sampled image values $f_n(k,l)$. This postfilter step, necessary for n>0, is decomposed in practice into a product of 2 1D functions applied in x and y; see [4,5] for the definition of the discrete postfilter and its implementation in terms of recursive filtering.

If we omit this last step and choose to display the coefficients image $C_{k,l}$ directly, we will end up with a smoothed version of the reconstructed image. This property can be of interest for reducing noise SPECT reconstructions [6].

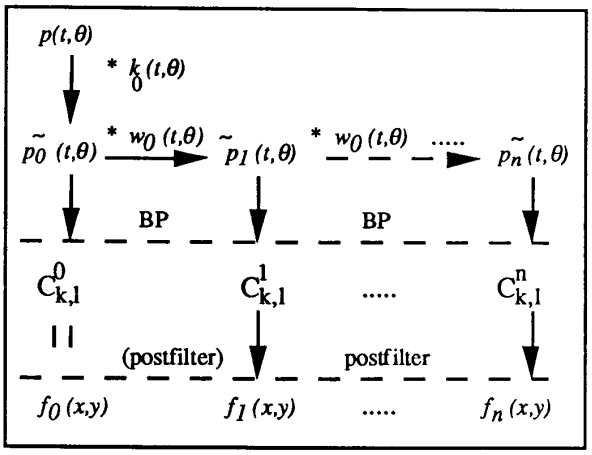


*Figure 3 : Reconstruction of $f_n(x,y)$ from $p(t,\theta)$*

Using Eqs. (31)-(33) an efficient implementation of the FBP, which gives each image (for i=0,1...n) corresponding to the degree of spline, can be realized and is summarized in Figure 3.

### *C. Discrete and continuous versions of $w_n(t,\theta)$*

The previous figure is valid only for the continuous case: even if the image has been sampled it is not the case of projections and kernel. The discretization of the kernel $w_0(t,\theta)$ convolved with itself does not give exactly the discrete kernel $w_1(t,\theta)$. More generally, we have :

$$w_n(t,\theta)\big|_{t=m} \neq w_0(m,\theta) * \underbrace{\ldots . * w_0(m,\theta)}_{\text{n times}} . \qquad (34)$$

The discretized version of this filter can be implemented using a cascade of moving average filters followed by an additional small correction kernel. The corresponding algorithm is described in details in [4].

### *D. Example of B-spline reconstruction*

Many experiments have already been done to check the properties of this algorithm. Discrete reconstructions exhibit good robustness to translational shift [2]. They do not have the 2D aliasing property inherent to the pixel sampling, and tend preserve edges better than the standard algorithm even in a noisy context [7]. For a SPECT device, the oversampling ratio $\rho$ was defined by the characteristics of the γ-camera : uncertainty of the position of the center of rotation and blur. The acquired signal is bandlimited and there is no reason to sample at a rate $\rho > 4$. Since $\rho = 4$ is also the low bound for the filtering step, this value has been retained for practical implementation.

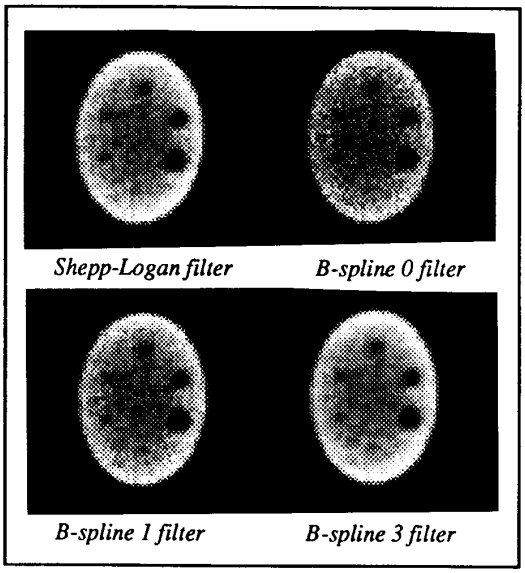


*Figure 4 : Reconstruction of a Jaszczack phantom*

Reconstructions of a Jazszcack phantom for the standard FBP with a Shepp-Logan filter and linear interpolation for the BP, and the spline reconstructions for n=0,1,2 and 3 have been done. For these experiments, we chose not to apply the postfilter. This process is in fact equivalent to lowpass filter the reconstructed image, which has the advantage of reducing the noise. The smoothing effect is more pronounced for higher

order splines and the representation of degree 2-3 is very close to the standard one. If one applies this last step (not shown here), the result will looks much more like the 0-1 degree B-spline images. More experiments and especially more specific detection tasks are to be defined fore an objective evaluation. We also need to address practical problems such as the distribution of counts per projection and the number of projection which give the "best" estimate of the object for a defined PIDM (see [6] for more details about the SPECT implementation).

## IV. DISCUSSION

The PIDM has the advantage of linking the continuous function with a discrete representation.
The use of spline PIDM suppresses 2D aliasing problems in the reconstruction. This is explained (using the oversampling of the projections) by the use of an optimal prefilter (the trapezoidal function $w_n$) on the projections before the sampling step in the reconstruction plane.

The spline FBP implementation does not suppress the angular artifacts but it acts differently than the standard FBP. It smears the singularity of the pixel edges along an angular sector, according to the shape of the discrete function $w_0$. Since this stability comes from the shape of the pixel, the connection with the Katz theory [8] for the angular sampling is direct : the numbers of pixels and the pixel vertices induce how to obtain the number of angles and their respective positions using a Farey series, in order to keep the maximum amount of information in the discrete projections. Another consequence is that, by modifying the shape of the pixel, the kernel behavior changes. The more the pixel shape tends to the disk, the higher the stability (the singularity is smeared all around the pixel). In our case, the use of hexagonal pixels would improve the stability of the 0-order reconstruction. For higher order, this singularity tends to disappear, as the angular variations.

The $V_0$ reconstruction is very different in terms of spatial-frequency content than the frequency-limited based reconstruction; its uses all the frequency information for a limited spatial representation. Increasing the order of spline basis generate different spectral contents for the representation of a pixel. Based on the asymptotic results in [5] and [9], it can be shown that the present procedure is equivalent to performing a bandlimited reconstruction as n tends to infinity. In the reconstruction case, this means that all the different solutions can be generated from the discrete filter derived in II-B.

The approach described here is also well suited for performing spline-based magnifications and reductions operations that can be described in terms of filters [4],[5]. In order to perform detection tasks onto a magnified part of a reconstruction, the consistency of the whole process, from the acquisition to the detection task, will be an important factor. The differences in terms of spatial-spectral content in these reconstructions will be analysed using this framework.

## V. ACKNOWLEDGMENTS

The authors want to acknowledge the help of A. AlDroubi and thanks K. Myers, R. Wagner and R. Gagne for their interest in this work, as well as their very helpful criticisms.
J-P Guedon is now with the Office for Science and Technology, CDRH/FDA under a National Research Council postdoc position.

## VI. REFERENCES

[1] J-P. Guedon and Y. Bizais, "Continuous and discrete Filtered Back-Projection.", submitted to IEEE Trans. in Medical Imaging, November 1991.

[2] J-P. Guedon and Y. Bizais, "Projection and Backprojection models and projection sampling in tomography.", *Proc. of SPIE Medical Imaging IV*, Vol 1231, pp.206-217, Newport Beach, CA, February 1990.

[3] R. Gagne, M. Anderson, "Geometrical, sampling and algorithmic aspects of Computed tomography." Annual meeting of the American Association of Physicists in Medicine, July 1988.

[4] M. Unser, A. Aldroubi, M. Eden, " Fast B-spline transforms for continuous image representation and interpolation.", *IEEE Trans. on Patt. Anal. Machine Intell.*, Vol. PAMI-13, No.3,p.277-285, March 1991.

[5] M. Unser, A. Aldroubi, M. Eden, "Polynomial spline signal approximations : filter design and asymptotic equivalence with Shannon sampling theorem.", to appear in *IEEE Trans. on Inf. Theory*, Vol.38, No.1, January 1992.

[6] J-P. Guedon, C. Barker, Y. Bizais, "B-spline FBP reconstruction for SPECT.", *Proc.* of the IEEE Nuclear Science Symposium, Santa Fe, NM, November 1990.

[7] J-P. Guedon, Y. Bizais, "Spline based regularisation for discrete FBP reconstruction.", *Proc. of the XIIth IPMI Conference*, ACF Colchester& DJ Hawkes eds, *Lect. Notes in Comp. Science*, Vol 511, Springer Verlag, pp. 59-67, 1991.

[8] Katz, *Questions of uniquness and resolution in reconstruction from projections, Lect. Notes in BioMath.* , Vol. 26, S. Levin Ed., Springer Verlag, 1978.

[9] A. Aldroubi, M. Unser, M. Eden, " Cardinal spline filters: stability and convergence to the ideal sinc interpolator.", NCRR Report 20/90, National Institutes of Health, 1990.

[10] D. Ludwig, " The Radon transform on Euclidean space.", Comm on Pure and Applied Mathematics, Vol XIX, pp. 49-81, 1966.